Formability evaluation for sheet metals under hot stamping conditions by a novel biaxial testing system and a new materials model

Shao, Zhutao; Li, Nan; Lin, Jianguo; Dean, Trevor

DOI:
10.1016/j.ijmecsci.2016.11.022

Document Version
Peer reviewed version

Citation for published version (Harvard):
Shao, Z, Li, N, Lin, J & Dean, T 2017, 'Formability evaluation for sheet metals under hot stamping conditions by a novel biaxial testing system and a new materials model', *International Journal of Mechanical Sciences*, vol. 120, pp. 149-158. https://doi.org/10.1016/j.ijmecsci.2016.11.022

Formability evaluation for sheet metals under hot stamping conditions by a novel biaxial testing system and a new materials model

Zhutao Shao, Nan Li, Jianguo Lin, Trevor Dean

www.elsevier.com/locate/ijmecsci

PII: S0020-7403(16)30892-X
DOI: http://dx.doi.org/10.1016/j.ijmecsci.2016.11.022
Reference: MS3501

To appear in: *International Journal of Mechanical Sciences*

Cite this article as: Zhutao Shao, Nan Li, Jianguo Lin and Trevor Dean Formability evaluation for sheet metals under hot stamping conditions by a novel biaxial testing system and a new materials model, *International Journal of Mechanical Sciences,* http://dx.doi.org/10.1016/j.ijmecsci.2016.11.022

Formability evaluation for sheet metals under hot stamping conditions by a novel biaxial testing system and a new materials model

Zhutao Shao[a], Nan Li[a*], Jianguo Lin[a], Trevor Dean[b]

[a]Department of Mechanical Engineering, Imperial College London, London SW7 2AZ, UK
[b]School of Mechanical Engineering, University of Birmingham, Edgbaston, Birmingham B15 2TT, UK

[*]Corresponding author. Tel: +442075949078. E-mail address: n.li09@imperial.ac.uk (Dr N. Li)

Abstract

Hot stamping and cold die quenching has been developed in forming complex shaped structural components of metals. The aim of this study is the first attempt to develop unified viscoplastic damage constitutive equations to describe the thermo-mechanical response of the metal and to predict the formability of the metal for hot stamping applications. Effects of parameters in the damage evolution equation on the predicted forming limit curves were investigated. Test facilities and methods need to be established to obtain experimental formability data of metals in order to determine and verify constitutive equations. However, conventional experimental approaches used to determine forming limit diagrams (FLDs) of sheet metals under different linear strain paths are not applicable to hot stamping conditions due to the requirements of rapid heating and cooling processes prior to forming. A novel planar biaxial testing system was proposed before and was improved and used in this work for formability tests of aluminium alloy 6082 at various temperatures, strain rates and strain paths after heating, soaking and rapid cooling processes. The key dimensions and features of cruciform specimens adopted for the determination of forming limit under various strain paths were developed, optimised and verified based on the previous designs and the determined heating and cooling method [1]. The digital image correlation (DIC) system was adopted to record strain fields of a specimen throughout the deformation history. Material constants in constitutive equations were determined from the formability test results of AA6082 for the prediction of forming limit of alloys under hot stamping conditions. This research, for the first time, enabled forming limit data of an alloy to be generated at various temperatures, strain rates and strain paths and forming limits to be predicted under hot stamping conditions.

Keywords Sheet metal forming, Hot stamping, Forming limit diagram (FLD), Biaxial testing, Formability prediction

1. Introduction

In automotive and aircraft industries, weight reduction can directly reduce energy consumption, which is beneficial to fuel economy improvement and environmental friendliness [2]. A 10% decrease in the mass of a conventional vehicle results in a 6% to 8% decrease in fuel consumption rate without compromising vehicle's performance [3]. Two feasible ways for reducing the weight of automobile structures are the use of high strength steel and the use of sheet of low density. At room temperature, high strength steel and aluminium alloys have low formability, which leads to high springback and poor surface quality of formed components. To deal with this problem, warm and hot forming technologies have been developed, which are hot stamping and cold die quenching (also termed as press hardening) for quenchable steel [4] and solution heat treatment, forming and in-die quenching (HFQ®) of lightweight alloys [5]. The hot stamping and cold die quenching process, abbreviated to hot stamping, is used to obtain shapes with great complexity and relatively high strength in automotive applications. In hot stamping process, heat treatable metal blank is heated up in a furnace, transferred to a press and subsequently formed and quenched in a cold tool [6]. The technique can be applied to both boron steel and low density sheet metals, such as aluminium alloys [7] and magnesium alloys [8]. It has been formulated as the HFQ® process, to form complex shaped parts for lightweight structure of vehicles. In the HFQ® process, a metal sheet is heated up to a specific temperature at which it is a solid solution with a single phase and then transferred to the press and subsequently formed and quenched in the cold tool [9, 10]. The control of forming conditions, such as heating rate, soaking time, cooling rate, forming temperature and strain rate, are critical for the success of these processes [11].

The forming limit diagram (FLD) is commonly used to evaluate the formability of sheet metals [12]. An FLD comprises a set of forming limit curve which identifies the boundary between uniform deformation and the beginning of plastic instability which leads to materials failure. According to the definition of an FLD, strain paths are described as proportional [13], from uniaxial through plane strain to equi-biaxial. The characteristic of path dependence causes an FLD to be invalid under non-proportional loading [14]. The FLD of a material at elevated temperatures vary greatly in terms of shape and position from one formed at room temperature. At an isothermal testing

condition, proportional strain paths and constant strain rates are required for the determination of FLD at elevated temperatures. Formability tests are used to obtain FLDs for sheet metals experimentally and two types of test method are conventionally used to determine forming limit strains, namely the out-of-plane test and the in-plane test. Nakazima test is a typical out-of-plane test [15], specimens with different widths are stretched by a hemispherical punch or hydraulic pressure [16]. Using multiaxial tube expansion test is an effective out-of-plane method to measure forming limits under various strain states and stress states [17]. The out-of-plane test at room temperature has been standardised. It has been used to obtain FLDs at elevated temperature as well [18]. Ayres et al. [19] investigated the effects of temperature and strain rate on the formability of AA5182 at a temperature of 130°C and 200°C. Bagheriasl [20] used cartridge heater for heating up the die in Nakazima test in order to obtain the FLDs of AA3003 at temperature of 100-350°C and strain rate of 0.003-0.1 /s. The digital image correlation (DIC) technique [21] was adopted for strain measurement during the tests. Min et al. [22] performed the formability test at a temperature of 800°C for boron steel to determine the left hand side of an FLD for hot stamping applications, but deformation temperature cannot be controlled accurately due to the transfer stage of specimen from a furnace to the cold tool. Shao et al. [23] determined FLDs for AA5754 at various temperatures (200-300°C) and forming speeds (20-300 mm/s) by setting up the test tool in a hot furnace to create an isothermal environment. In order to simulate HFQ® conditions, the requirement to simultaneously form and quench after heating makes testing in a furnace impractical. In the in-plane test, such as the Marciniak test [24], the test material is stretched over a flat-bottomed punch of cylindrical/elliptical cross section. A carrier blank with a central hole is usually used to avoid frictional contact between the sheet metal specimen and the punch, but optimising the dimension and geometries of carrier blank and punch is required in order to induce strain localisation and cracking in the unsupported region of the specimen, which complicates the test procedure and increases the cost of testing. Li and Ghosh [25] carried out a formability test of aluminium alloys 5754, 5182 and 6111 by using the Marciniak approach at a rapid forming rate of 1 /s and a range of temperature of 200–350°C, but data was not obtained at temperatures over 350°C. Naka et al. [26] investigated the effects of forming speed (0.2-200 mm/min corresponding to strain rate of 0.0001-0.1 /s) and temperature (20-300°C) on forming limits for AA5083 by using a heated punch in the

in-plane test. Planar tensile tests utilising a tensile machine with a cruciform specimen is an alternative method to determine forming limits of a material. Hannon and Tiernan [27] reviewed planar biaxial testing systems for sheet metals. Two types of test machines are generally used, i.e. stand-alone biaxial tensile test machines and link mechanism attachments in uniaxial test machines for biaxial testing. Leotoing et al. [28] improved a cruciform specimen for the use of formability tests and determined the FLD of AA5086 at room temperature [29]. A servo-hydraulic biaxial testing machine was used to control loading paths in two vertical directions [30]. A better linearity of strain path can be obtained by a planar biaxial testing machine compared to conventional Nakazima and Marciniak tests. Abu-Farha et al. [31] investigate biaxial deformation of AA5083 and AZ31 at 300°C by using a designed testing tool and a heat gun based on an INSTRON uniaxial tensile test machine.

However, neither of the out-of-plane and the in-plane methods discussed above for determining forming limits are suitable for hot stamping applications because extra heating and cooling devices are needed and control of heating rate, cooling rate, deformation temperature and stretching strain rate is difficult to obtain precisely. Therefore, a formability testing system was proposed previously to determine FLDs of alloys experimentally under hot stamping conditions.

Experimentally determining formability is time-consuming and costly, which restricts the number of tests that may be conducted. Because of that, various analytical and numerical models have been developing as an alternative to perform theoretical formability prediction and eliminate the need for much experimental work. Banabic et al. [32] and Stoughton et al. [33] reviewed primary models for forming limit prediction at room temperature from four aspects, namely new constitutive equations used for limit strain computation, polycrystalline models, ductile damage models, advanced numerical models for non-linear strain path or various process parameters. Theoretical models applied to FLD prediction at elevated temperature include Hora's theory [34, 35], M-K theory [24, 36, 37] and Storen and Rice's theory Rice [22, 38, 39]. Although various analytical and numerical models have been developed for theoretical formability prediction, most of them are applicable to ambient conditions or warm/hot forming conditions. Viscoplasticity theory can also be used for analysis on forming processes at elevated temperatures and a dislocation-based viscoplastic-

damage model had been proposed by Lin et al. [40] since microstructural evolution at elevated temperatures has a great effect on formability of an alloy. This theory can be developed to predict forming limits of metals for hot stamping applications [41].

The goal of this paper is to employ improved biaxial test system and optimised specimens to enable experimental data of FLDs of an alloy, for the first time, to be determined under hot stamping conditions, and to be used for calibration of materials model. A novel planar biaxial testing system for use on a Gleeble thermo-mechanical simulator is presented first in this paper to obtain FLDs of AA6082 under HFQ® conditions. Formability tests of AA6082 were conducted at various temperatures, strain rates and strain paths after heating and cooling processes. A 2D continuum damage mechanics (CDM)-based material model was developed for the prediction of forming limit of alloys under HFQ® conditions and the constitutive equations were calibrated from the formability test results of AA6082.

2. Experimental programme

2.1 Temperature profile

Hot stamping conditions contain the control of heating rate, soaking time, cooling rate, deformation temperature and strain rate. Aluminium alloy 6082, which is extensively used in the automotive industry [42], was used to machine the specimens to conduct the formability tests under HFQ® conditions. Chemical composition of commercial AA6082 at T6 condition is shown in Table 1. The determination of FLDs requires the deformation of the specimen to be performed at constant temperature and constant strain rate under different linear strain paths. A schematic of the required temperature profile for formability tests of AA6082 under HFQ® conditions is shown in Fig. 1. Heating rate and cooling rate are critical parameters for the HFQ® process and should be controlled precisely to maintain a supersaturated solid solution without grain degradation in a specimen. The material of AA6082 was heated to the solution heat treatment temperature of 535°C [43] at a heating rate of 30 °C/s, soaked for 1 minute, which was sufficient for full resolution of precipitates, and then quenched to a designated temperature in the range of 370-510°C at a cooling rate of 100 °C/s [44]. The tensile tests were conducted at constant strain rates in the range of 0.01-1 /s. The input displacement to the biaxial test was calculated before testing according to the designated strain rate and it can be controlled accurately by the Gleeble to enable a

constant true strain rate of the specimen to be obtained at the concerned central region during deformation until the onset of necking. Strain path condition contains uniaxial, plane strain and biaxial testing. At least three tests were completed for each test condition and each strain path to prove the repeatability.

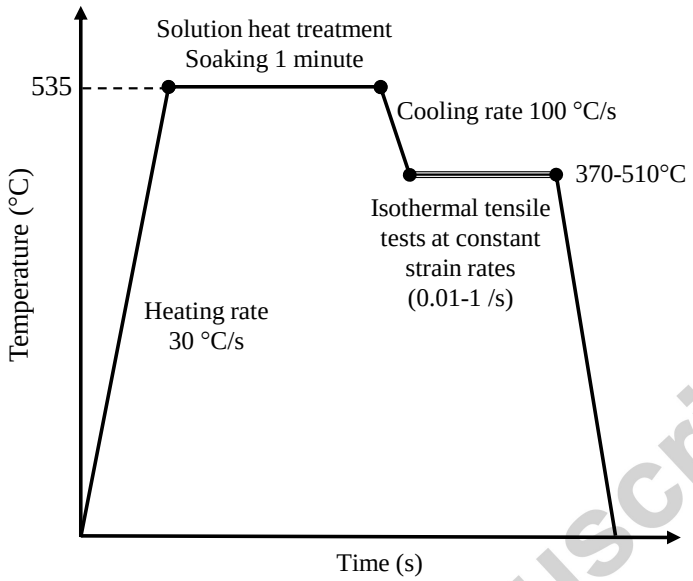

Fig. 1 A schematic showing the temperature profiles for obtaining forming limit data of AA6082 under HFQ® conditions.

Table 1 Chemical composition of AA6082

Element	Si	Fe	Cu	Mn	Mg	Cr	Zn	Ti	Al
Weight proportion (%)	0.90	0.38	0.08	0.42	0.70	0.02	0.05	0.03	Balance

2.2 Design of a biaxial testing apparatus

The core part of the novel biaxial testing system is the biaxial mechanism, which was designed to be used on a Gleeble 3800 [45]. The test apparatus was used to convert an input uniaxial force from a Gleeble into an output biaxial force of different loading ratios by coupling two rotatable plates to a central drive shaft, so that different strain paths were realised. A specimen can be clamped on top of the biaxial mechanism. Detailed descriptions of the biaxial mechanism can be found in the previous study [1].

Advantageously, this mechanism is relatively simple and is employable within limited space on tensile test machines. The heating and cooling rates can be controlled accurately by a Gleeble so that complex forming conditions can be applied. Friction effect on the FLD of a material is avoided. Based on the proposed planar biaxial apparatus, strain states can be controlled and different strain paths can be obtained so that an FLD can be obtained under hot stamping conditions.

2.3 Set-up of biaxial tensile testing

Fig. 2 is the set-up of the experimental system on the Gleeble 3800. The DIC system with a high-speed camera and a micro lens was used for strain measurement and this technique enables full-field strains to be measured at different stages by comparing the digital images of a pattern sprayed on a specimen. Different framing rates were used to correspond with different experimental stretching strain rates. In this work, for the tests at strain rates of 0.01 /s, 0.1 /s and 1 /s, the framing rates were used as 25 fps, 50 fps and 500 fps for full resolution of 1280×1024 pixels, respectively. The high-speed camera was triggered after heating and cooling processes to start to record images during the stretching of a specimen. ARAMIS, a non-contact optical 3D deformation measuring system, was used to record the deformation history during the deformation of a specimen and to post-process images for the determination of forming limit strain. Facet size of 10 pixels and facet step of 8 pixels were used for the post-processing analysis in order to obtain sufficient grids for the determination of forming limits according to the standard analysis procedure in ARAMIS.

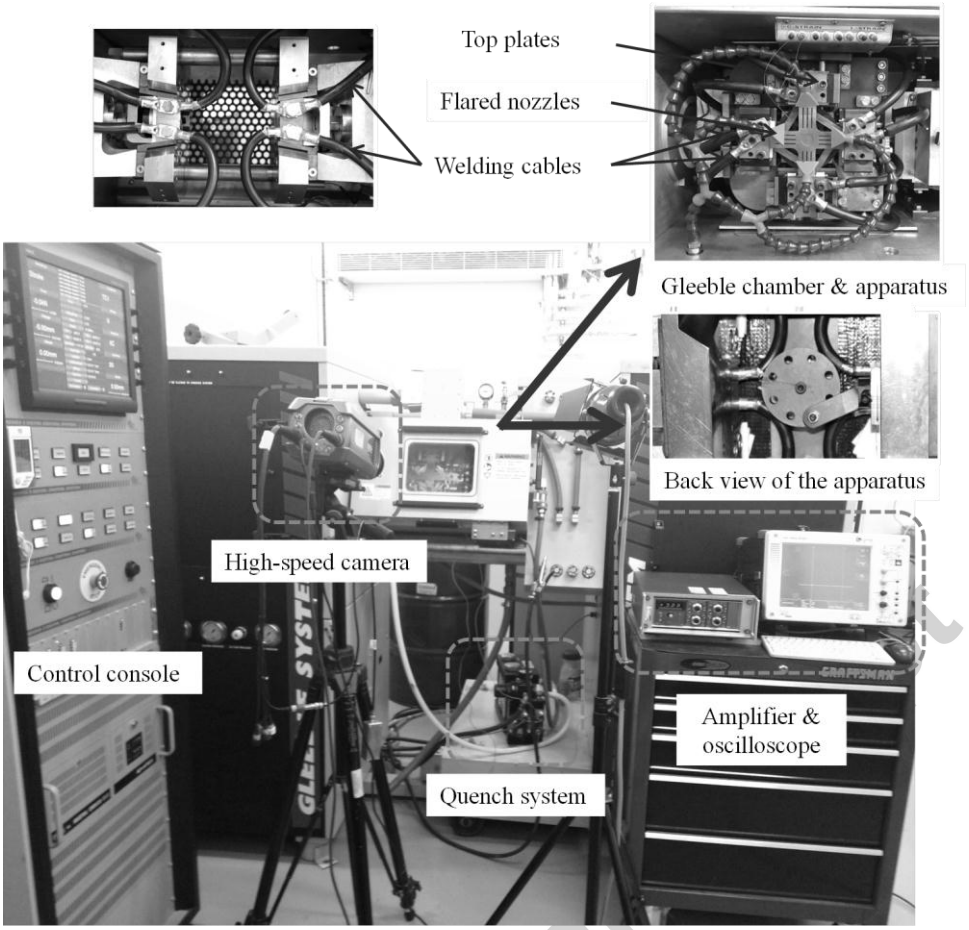

Fig. 2 The set-up of the biaxial testing system for formability tests

The top surface of a cruciform specimen faced and was close to the camera lens. The micro camera lens was adjusted to be parallel to the specimen surface by checking whether the quality of camera focus is consistent on each corner of the captured image on a computer screen. The pattern with black background and white dots was pre-painted on the surface of the specimen and, by using the FlameProof spray, the pattern does not degrade at temperatures below 1093°C which is lower than the maximum required temperature of 535°C. Thermocouples are attached to the backside of the specimen and linked to the Gleeble temperature control system in order to monitor temperature history on a specimen.

Each of four clamping regions on one arm of a cruciform specimen contacted tightly with a stainless steel plate which is electrode for resistance heating. Cables with crimp ring terminals were used to connect the plates to the power supply of the Gleeble for resistance heating. Two adjacent arms of a cruciform specimen are connected to positive electrodes and the other two arms are attached to negative electrodes and

electrical current goes through the entire specimen to heat it. The quench system with a maximum regulated air of 120 psi connected to four flared nozzles for air cooling. Cooling air can envelop the entire gauge region of the specimen and cooling rate of 100°C/s can be obtained by applying half of the regulated air pressure in this study.

3. Development of specimen design

3.1 Dimensions of specimens

Various cruciform specimens with different features were designed for biaxial testing [27, 46, 47] in order to characterise mechanical behaviour of metals subjected to biaxial loading, as shown in Fig. 3, but no standard of cruciform specimen geometry for biaxial testing has been developed and no existing specimens can be used directly in the new biaxial apparatus because of the usage of resistance heating. The objective of specimen design is to ensure that the beginning of localised necking starts within the central biaxial loading region of a specimen instead of in the arms.

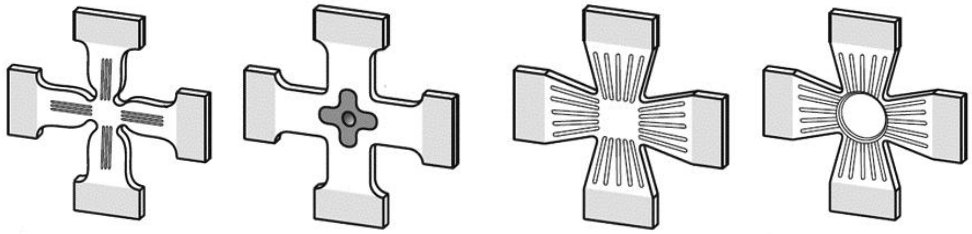

(a) (b) (c) (d)

Fig. 3 Cruciform geometries with features of slots and central thickness reduction used in different biaxial testing studies [30]

For a cruciform specimen, the arms experience uniaxial tension while the central region is tensioned biaxially. The load bearing capacity of sheets under uniaxial tension is smaller than that under biaxial tension so that failure usually occurs in the arms of a cruciform specimen in a biaxial testing. It has been found that thickness reduction in the central region and slots in the arms of a cruciform specimen are beneficial for both inducing localised necking to occur in the central gauge region and improving the uniformity of strain and stress distribution [48-50]. In this case, only the central zone is considered as the gauge section where biaxial loading condition is fulfilled. Therefore, the features of thickness reduction and slots in the arms were

adopted in this work for the specimen design. A series of specimen designs with different shapes and dimensions of gauge section, slots and fillets were evaluated based on extensive experimental trials and finite element simulations. The criteria for optimisation were the uniformity of temperature field and strain field at gauge section, linear strain path control and failure location control. The optimum designs of specimens, for different tensile conditions, are given in Fig. 4.

Fig. 4(a) shows a flat dog-bone specimen with a 98 mm parallel length used for formability tests of AA6082 under uniaxial tension state for HFQ® conditions. The thickness of the uniaxial testing specimen was 1.5 mm. Fig. 4(b) shows the dimensions of cruciform specimen used for equi-biaxial testing. Fillets of 10 mm exist between two opposing corners of the cruciform specimen to reduce stress concentration in the corners and the value was reduced to 2 mm for the other two opposing corners in order to balance the temperature asymmetry in the arms of the specimen. The thickness of central circular gauge zone was reduced to 0.7 mm from 1.5 mm through recessing each surface by 0.4 mm. This was designed to undergo recorded deformation under biaxial stretching in the concerned central region. Since the deformation will take place after heat treatment process of the material during testing, any possible strain hardening caused during machining would be eliminated through dislocation recovery; therefore, the effect of thickness reduction on the results was not considered in this research. Slots with the width of 1.4 mm and the length of 28 mm were machined into the arms by laser cutting for distributing the load uniformly to the central gauge region. The distance from the mid-length of the cruciform specimen to the ends of the slots in arms is 15.5 mm. Fig. 4(c) shows the cruciform specimen used for plane strain testing. Only one slot exists in two loaded arms for this geometry and the middle slot is 1.5 mm shorter than others in the other two arms. Fillets of 10 mm are at the intersection of two adjacent arms and other dimensions of the specimen are shown in Fig. 4(c).

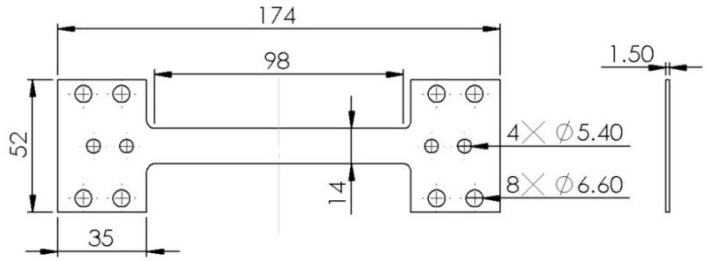

(a) Dimensions of the uniaxial specimen

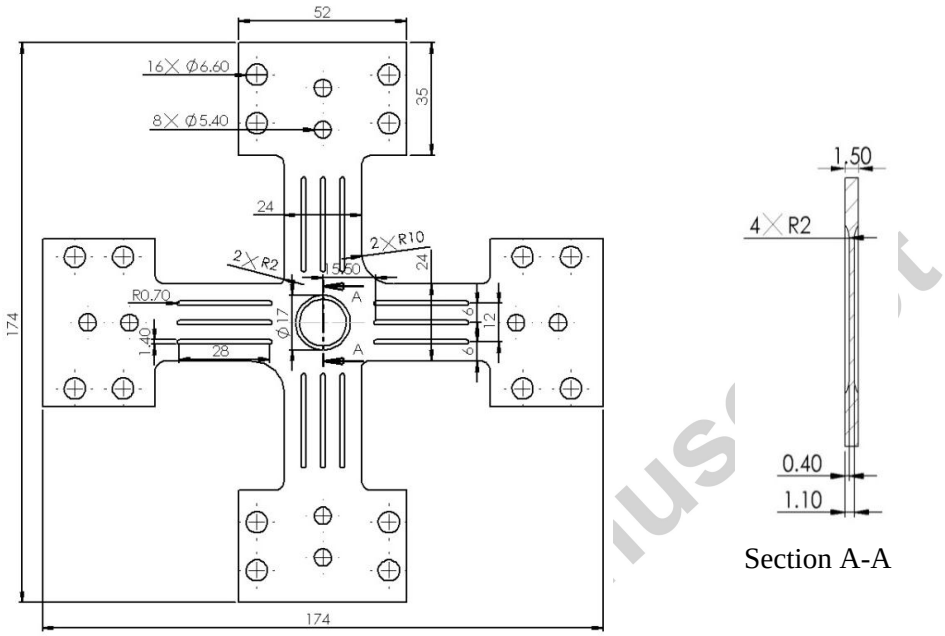

(b) Dimensions of the cruciform specimen for equi-biaxial testing

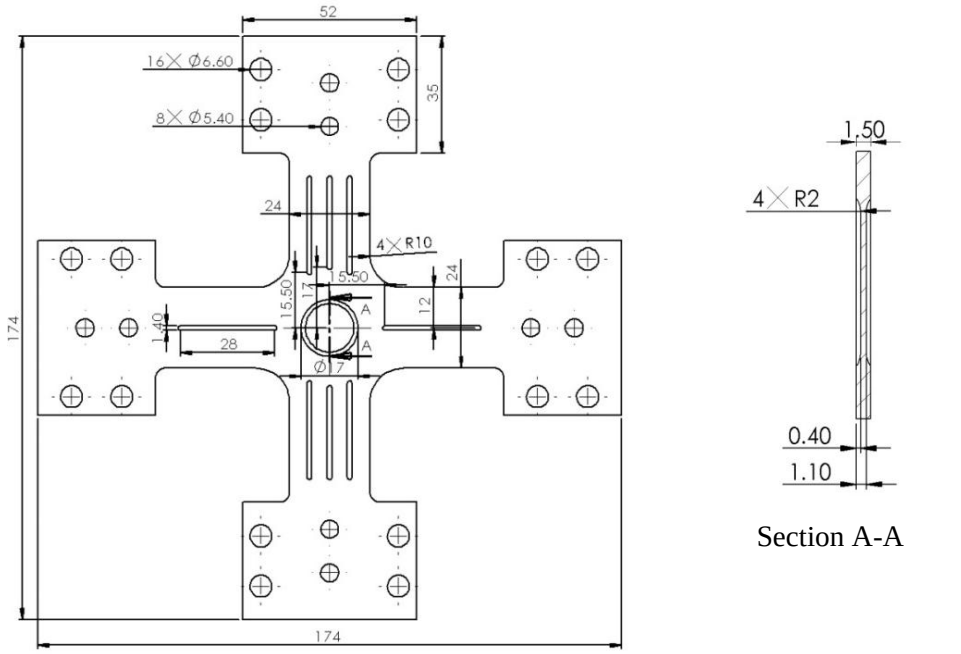

(c)Dimensions of the cruciform specimen for plane strain testing

Fig. 4 Dimensions (in mm) of specimens used for the formability test

3.2 Experimental verification

Some dimensions of the specimen have been modified, which has observable effect on the temperature distribution of a specimen due to resistance heating; therefore, the updated designs have to be verified again. Experiments were conducted to measure the temperature distribution in an specimen subjected to solution heat treatment under HFQ® conditions, by using selective heating and cooling method. A few pairs of thermocouples were welded on the surface of each specimen in order to identify temperature gradients. In Fig. 5, the locations of the thermocouples are marked and 6 locations on the specimen are identified in Fig. 5(a) for the equi-biaxial testing and 4 locations in Fig. 5(b) for the plane strain testing. The temperature at central location 1 was controlled precisely by the Gleeble. The specimens were heated up to 535°C at the central point, soaked for 1 min, and then cooled to 440°C and soaked for 15 seconds. The average values at soaking time at temperatures of 535°C and 440°C were calculated, as shown in Table 2. A similar temperature history at each location of thermocouples can be seen from previous study [1]. A higher temperature within the central gauge region of a cruciform specimen is beneficial for inducing failure to start in this area. For the specimen used for equi-biaxial testing, the temperature difference within the central concerned region was within ±10°C when the temperature at central location remained at 440°C. Since the gradient of electrical potential decreases from the positive electrodes to the negative electrodes in the specimen, temperature distribution out of the gauge region was not symmetric, which may have effects on the deformation of the central zone and the value of the ratio of minor strain to major strain. For the cruciform specimen used for plane strain testing, the maximum temperature difference within the central concerned region was within ±5°C when the temperature at central point remained at 440°C. The specimen geometry determines the variation of temperature along the entire specimen due to resistance heating; however, acceptable uniformity of temperature distribution within the concerned central zone of both designs was successfully obtained.

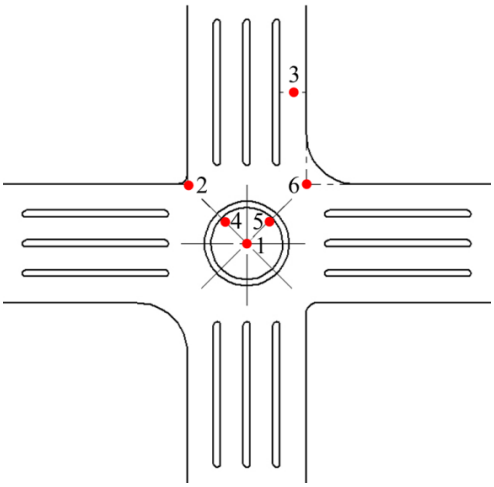

(a) 6 locations of thermocouples welded on cruciform specimen for the equi-biaxial testing condition

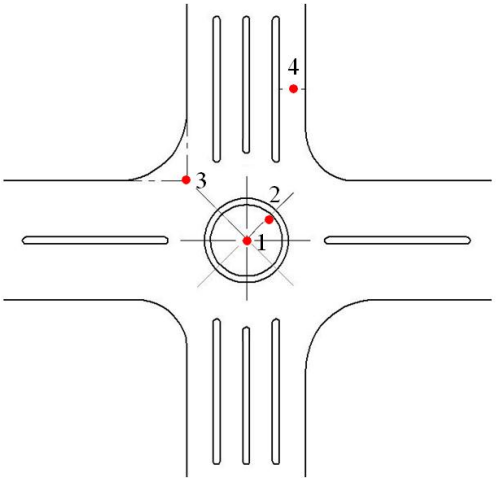

(b) 4 locations of thermocouples welded on cruciform specimen for the plane strain testing condition

Fig. 5 Locations of thermocouples welded on geometries

Table 2 Experimental results of temperatures at different locations on geometries

Temperature results (°C)	T1	T2	T3	T4	T5	T6
Specimen for equi-biaxial testing	535.03	503.13	493.28	522.22	540.51	549.61
	439.98	423.82	408.64	431.11	445.46	451.31
Specimen for plane strain testing	535.02	540.78	505.24	503.53		
	439.42	444.12	422.64	423.70		

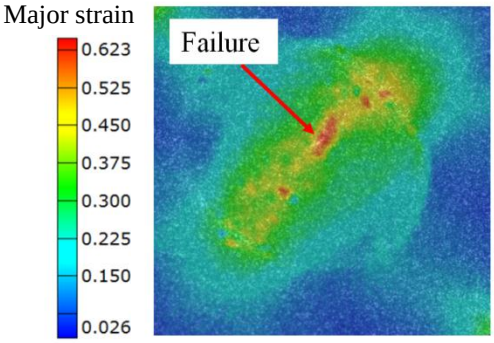

(a) Fracture of cruciform specimen under the equi-biaxial state

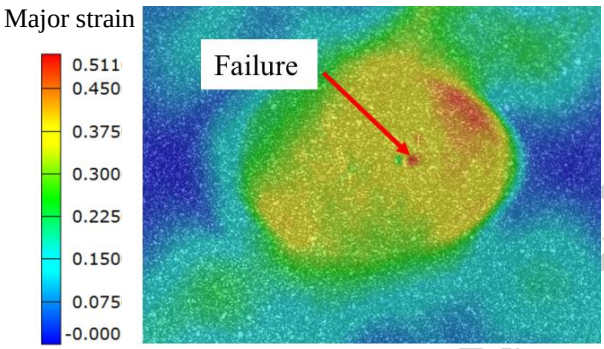

(b) Fracture of cruciform specimen under the plane strain state

Fig. 6 Experimental validation of the cruciform specimen designs, through DIC measurement, at the deformation temperature of 440 °C and the strain rate of 0.1 /s

The equi-biaxial testing was performed using the proposed cruciform specimens at the deformation temperature of 440°C and at the strain rate of 0.1 /s after solution heat treatment at 535°C and quenching. Fig. 6 shows the DIC results of biaxial tensile tests before failure by using specimen for equi-biaxial testing and plane strain testing, respectively. The international standard ISO 12004-2 [51] was used to identify the onset of necking and thus determine forming limit. This method was already embedded in the ARAMIS software. The principle of this standard method is to analyse the measured strain distribution along predefined cross sections which are perpendicular to the crack direction. An inverse parabola was fitted through two fit windows, which were determined using the second derivative of the strain values against their positions, on both sides of the crack. The values of peak points on the fitted curve were used as the limit major strain and limit minor strain. The ratio of strain path (minor strain to major strain) is 0.307 in Fig. 6(a) and that is 0.132 in Fig. 6(b). Higher values of strain level can be observed in the central gauge region than in

surrounding regions, which indicate the location of failure. The failure locations were observed in the central zones experimentally for equi-biaxial and plan strain testing, which verified the design of both cruciform specimens for formability testing.

4. Experimental results of uniaxial/biaxial formability testing

The linearity of strain path for each experimental test condition was investigated since FLD is highly strain path dependent. Representative results of strain paths are shown in Fig. 7. The data was collected from the fracture region instead of the central point of the specimen through the DIC results and at least 5 points were chosen to calculate the average values of major strain and minor strain. The actual strain rate was measured through data processing (by calculating the slope of true strain with deformation time) and was correlated with the designed strain rate. The linear fits are also shown in this figure. It can be seen that the strain paths are approximately proportional throughout deformation for each test condition, so that strain path linearity was achieved.

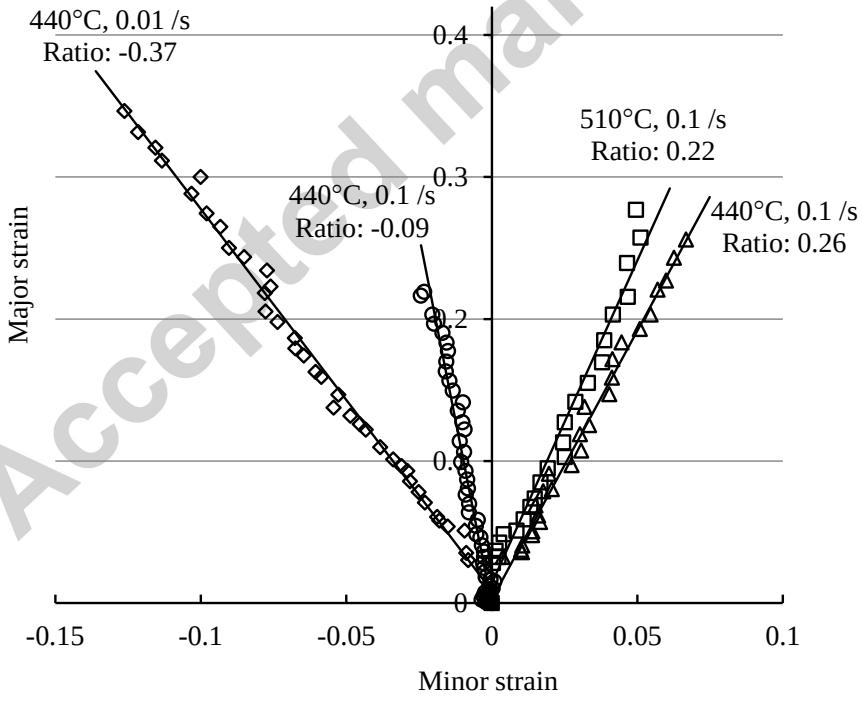

Fig. 7 Evolution of strain paths for various testing conditions

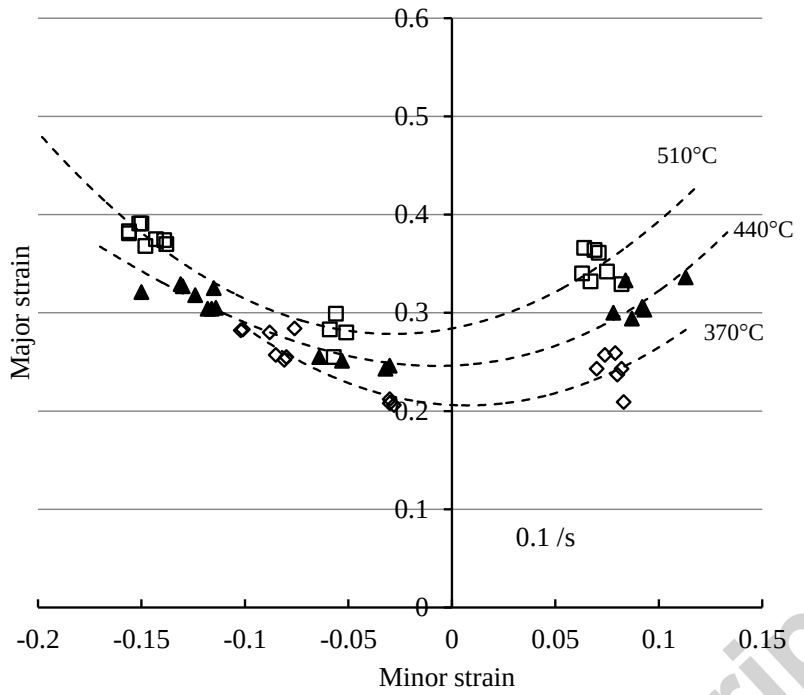

(a) FLD for different deformation temperatures at 0.1 /s

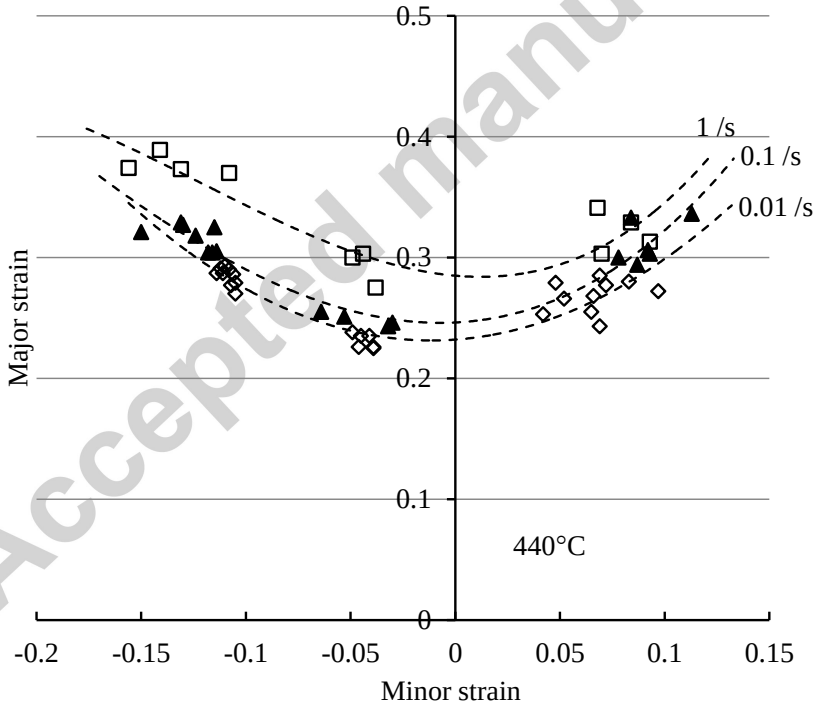

(b) FLD for different strain rates at 440°C

Fig.8 FLDs of AA6082 at various deformation temperatures and strain rates under hot stamping conditions (Dashed lines were obtained through the polynomial fitting algorithm)

By processing data for different geometries of specimens stretched under different strain states, forming limit data of AA6082 for different strain paths, under different temperatures and strain rates, was determined and shown as symbols in Fig. 8. Dashed lines in Fig. 8 were obtained through the polynomial fitting algorithm. The FLDs of AA6082 for HFQ® conditions could be obtained through curve fitting by a material model, shown as solid curves in the figure (details on the materials model are given in Section 5). In Fig. 8 (a), a monotonic increase is observed in forming limit from the temperature of 370°C to 510°C. It indicates that high formability of AA6082 can be obtained at a higher temperature under HFQ® conditions. The three forming limit curves are quite close to each other on the left hand side of the FLD, which means that the sensitivity of temperature dependence is larger for tension-tension biaxial strain paths than for tension-compression strain paths. It is found that when the strain rate increases from the designated strain rate of 0.01 /s to 1 /s, the forming limit of AA6082 increases, as shown in Fig. 8(b). The forming limit has a larger increase from 0.1 /s to 1 /s than that from 0.01 /s to 0.1 /s. In summary, higher forming speeds and higher temperatures within the designated ranges are beneficial for enhancing the forming limits of AA6082 under HFQ® conditions. This founding is consistent with that of the uniaxial tensile test of AA6082 [52] under hot stamping conditions. It was found that strain hardening increases with increasing strain rate (0.1-4 /s) and decreasing temperature (400-500°C). Ductility decreases with decreasing temperature and decreasing strain rates in the range of 0.01-1/s.

5. 2D Continuum damage mechanics (CDM)-based materials model

5.1 Constitutive equations

In order to predict an FLD of sheet metals under hot stamping conditions, a 2D CDM-based materials model was developed, which comprises a set of equations describing the viscoplastic behaviour of the material. These viscoplastic equations are expected to capture the features of forming limit curves of sheet metals under various thermo-mechanical conditions. By considering von-Mises behaviour for rigid perfect viscoplasticity, a power-law viscoplastic potential function ψ can be defined in the form of [53]:

$$\psi = \frac{K}{n+1}\left(\frac{\sigma_e}{K}\right)^{n+1} \tag{1}$$

where K and n are material constants. σ_e ($\sigma_e = \left(\frac{2}{3}S_{ij}S_{ij}\right)^{1/2}$) is the von-Mises stress, where S_{ij} ($S_{ij} = \sigma_{ij} - \sigma_{kk}\delta_{ij}/3$) are the deviatoric stresses, σ_{ij} is stress tensor and δ_{ij} is the Kronecker delta. The following expression can be obtained by differentiating the Eqn. (1) in terms of the deviatoric stresses:

$$\dot{\varepsilon}_{ij}^{P} = \frac{\partial \psi}{\partial S_{ij}} = \frac{3}{2}\frac{\partial \psi}{\partial \sigma_e}\frac{S_{ij}}{\sigma_e} = \frac{3}{2}\frac{S_{ij}}{\sigma_e}\left(\frac{\sigma_e}{K}\right)^{n} = \frac{3}{2}\frac{S_{ij}}{\sigma_e}\dot{\varepsilon}_e \tag{2}$$

where $\dot{\varepsilon}_e$ is effective strain rate.

Based the previous studies [41, 54], a set of unified viscoplastic constitutive equations are formulated as below:

$$\dot{\varepsilon}_e = \left(\frac{\left|\frac{\sigma_e}{1-\omega}\right| - R - k}{K}\right)^{n_1} \tag{3}$$

$$\dot{\varepsilon}_{ij}^{P} = \frac{3}{2}\frac{S_{ij}}{\sigma_e}\dot{\varepsilon}_e \tag{4}$$

$$\dot{R} = 0.5B\bar{\rho}^{-0.5}\dot{\bar{\rho}} \tag{5}$$

$$\dot{\bar{\rho}} = A(1-\bar{\rho})|\dot{\varepsilon}_e| - C\bar{\rho}^{n_2} \tag{6}$$

$$\sigma_{ij} = (1-\omega)D_{ijkl}\left(\varepsilon_{ij} - \varepsilon_{ij}^{P}\right) \tag{7}$$

$$\dot{\omega} = \left[\frac{\Delta^*}{(\mu_1 - 0.5\mu_2)^{\phi}}\right]\left(\frac{\mu_1\varepsilon_1 + \mu_2\varepsilon_2}{\gamma + \varepsilon_P}\right)^{\phi}\frac{\eta_1}{(1-\omega)^{\eta_3}}(\dot{\varepsilon}_e)^{\eta_2} \tag{8}$$

where the temperature dependent parameters in Eqns. (1)-(8) are defined by:

$$\boldsymbol{K = K_0 \exp\left(\frac{Q_K}{R_g T}\right)} \tag{9}$$

$$\boldsymbol{k = k_0 \exp\left(\frac{Q_k}{R_g T}\right)} \tag{10}$$

$$n_1 = n_{1_0} \exp\left(\frac{Q_{n1}}{R_g T}\right) \tag{11}$$

$$B = B_0 \exp\left(\frac{Q_B}{R_g T}\right) \tag{12}$$

$$C = C_0 \exp\left(-\frac{Q_C}{R_g T}\right) \tag{13}$$

$$\boldsymbol{\eta_1 = \eta_{1_0} \exp\left(-\frac{Q_{\eta 1}}{R_g T}\right)} \tag{14}$$

$$\boldsymbol{\eta_2 = \eta_{2_0} \exp\left(\frac{Q_{\eta 2}}{R_g T}\right)} \tag{15}$$

$$\eta_3 = \eta_{3_0} \exp\left(\frac{Q_{\eta 3}}{R_g T}\right) \tag{16}$$

$$E = E_0 \exp\left(\frac{Q_E}{R_g T}\right) \tag{17}$$

$$\mu_1 = \mu_{11} \exp\left(-\frac{\mu_{12}}{T}\right) \tag{18}$$

$$\phi = \phi_{11} \exp\left(-\frac{\phi_{12}}{T}\right) \tag{19}$$

$$\Delta^* = \Delta_{11}^* \exp\left(\frac{\Delta_{12}^*}{T}\right) + \Delta_{21}^* \exp(\Delta_{22}^* \dot{\varepsilon}_e) \tag{20}$$

where R_g is the universal gas constant, T is the absolute temperature. A, n_2, K_0, k_0, n_{1_0}, B_0, C_0, η_{1_0}, η_{2_0}, η_{3_0}, E_0, Q_K, Q_k, Q_{n1}, Q_B, Q_C, $Q_{\eta 1}$, $Q_{\eta 2}$, $Q_{\eta 3}$, Q_E, μ_{11}, μ_{12}, μ_2, γ, ϕ_{11}, ϕ_{12}, Δ_{11}^*, Δ_{12}^*, Δ_{21}^* and Δ_{22}^* are material constants to be determined from experimental data.

Eqn. (3) is the flow rule, in which effective strain rate $\dot{\varepsilon}_e$ is formulated by using the traditional power law with damage ω taken into account. k is the initial yield point and R represents the isotropic hardening. R in Eqn. (5) is a function of the normalized dislocation density $\bar{\rho}$ ($\bar{\rho} = 1 - \rho_0/\rho$, where ρ_0 is the initial dislocation density and ρ is the instantaneous dislocation density during deformation), where $\bar{\rho}$ is given by Eqn. (6). Eqn. (6) represents the accumulation of dislocations due to plastic flow, and dynamic and static recovery. The effect of damage ω was introduced in flow stress Eqn. (7), where D_{ijkl} is the elastic matrix of a material. In Eqn. (8), the damage evolution $\dot{\omega}$ was based on the nucleation and the growth of voids around particles. It is a modified version of the expression set out by Khaleel et al. [55] for damage due to superplastic void growth, which is appropriate for this case where the fine grained alloy is deformed by a significant amount at high temperature [7]. Since a typical forming limit curve is the plot of minor strain and major strain under different strain paths, the first two terms in Eqn. (8) are proposed to describe the effects of strain states on the damage evolution in the material. The parameters μ_1 and μ_2 are used to calibrate the effects of major strain and minor strain on the damage evolution. The values of $\mu_1$and μ_2 are suggested to be in the range of 0-1.0. ϕ is introduced in Eqn. (8) to control the intensity of the effects of principal strains on the damage evolution, thus to control the predicted FLD of a material. μ_1 and ϕ are defined as temperature dependent and Δ^* is defined as both temperature dependent and strain rate dependent, given in Eqns. (18)-(20).

5.2 Effects of parameters on predicted curves

Fig.9 shows the effect of the correction factor Δ^* on the position of a forming limit curve at the deformation temperature of 440°C and the strain rate of 0.1 /s. When the value of Δ^* varies from 0.5 to 2.0 with fixed other parameters (ϕ, μ_1 and μ_2), the location of a forming limit curve becomes lower but no significant changes of shape are observed. The coverage range of the values of forming limit under each strain path becomes larger and the lowest point of the curve moves towards the left hand side of

the FLD when a lower value of Δ^* is adopted in the damage evolution equation. The values of forming limit may vary depending on the particular experimental test method used. Therefore, Δ^* is also considered as a correction factor for adjusting predicted results and fitting to experimental data.

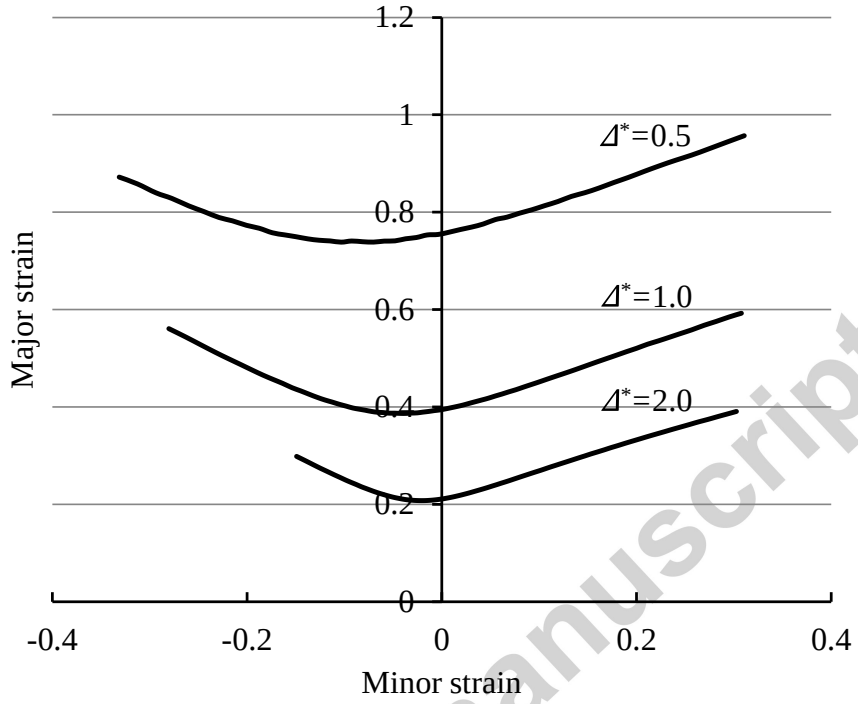

Fig. 9 The effect of the correction factor $\boldsymbol{\Delta^*}$ on the predicted curve at the deformation temperature of 440°C and the strain rate of 0.1 /s (Ø=5.60, $\boldsymbol{\mu_1}$=0.45, $\boldsymbol{\mu_2}$=0.15)

Fig.10 and Fig. 11 show the effects of the significance of major strain and minor strain on the shape of a forming limit curve, respectively, under the same condition of the deformation temperature of 440°C and the strain rate of 0.1 /s. A small range of μ_2 value causes a dramatic change of the curve shape, which means that μ_2 is a more sensitive parameter than μ_1. The effects of the two parameters μ_1 and μ_2 on the shape of a forming limit curve are quite similar. The strain level on the right hand side of the FLD and the location of the lowest point of a curve can be adjusted by varying the values of μ_1 and μ_2 to model the effects of principal strains on the damage evolution. A low value of μ_1 and a high value of μ_2 contribute to increasing the damage evolution rapidly.

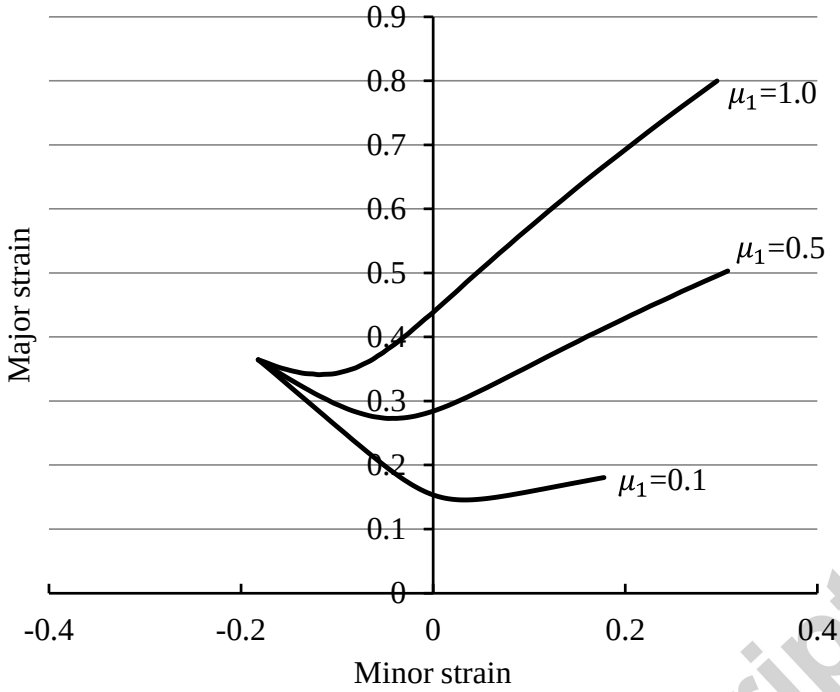

Fig. 10 The effect of the major strain parameter $\boldsymbol{\mu_1}$ on the predicted curve at the deformation temperature of 440°C and the strain rate of 0.1 /s ($\boldsymbol{\Delta}^*$=1.60, ∅=5.6, $\boldsymbol{\mu_2}$=0.15)

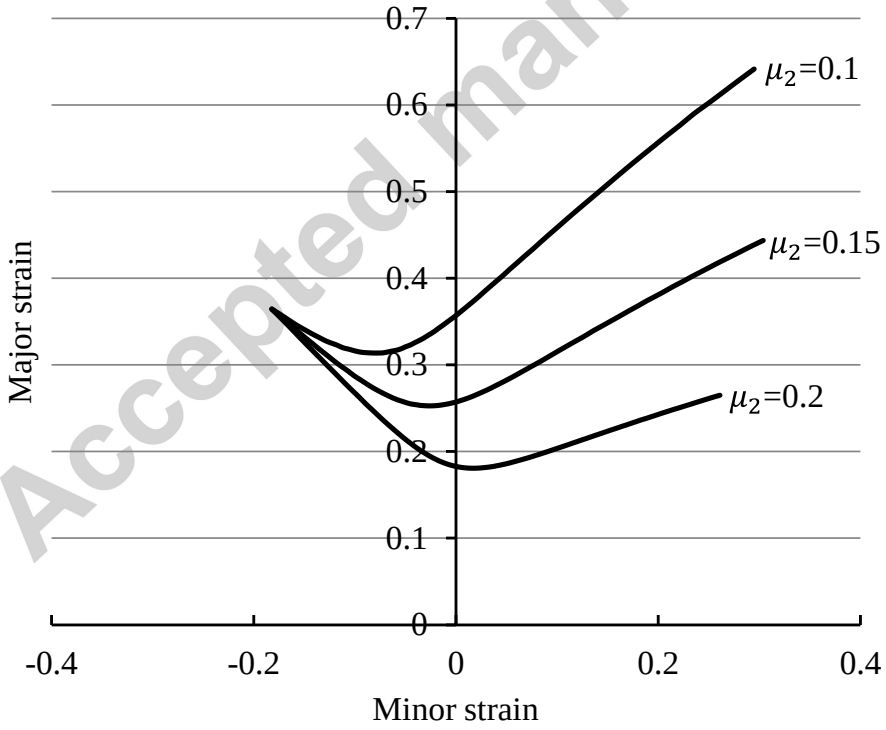

Fig. 11 The effect of the minor strain parameter $\boldsymbol{\mu_2}$ on the predicted curve at the deformation temperature of 440°C and the strain rate of 0.1 /s ($\boldsymbol{\Delta}^*$=1.60, ∅=5.6, $\boldsymbol{\mu_1}$=0.45)

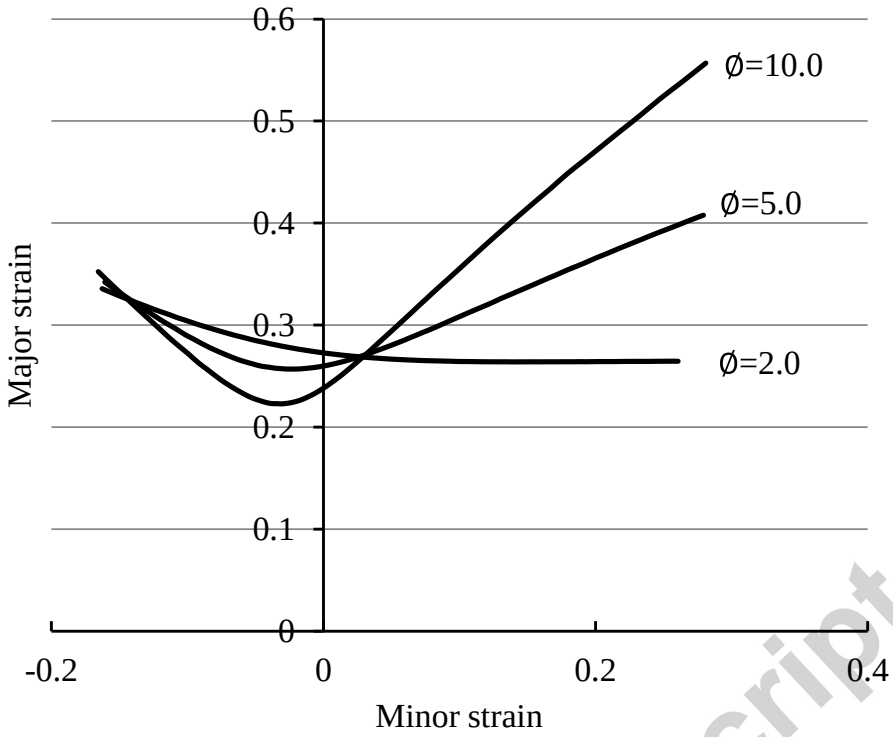

Fig. 12 The effect of the damage rate exponent $\boldsymbol{\phi}$ on the predicted curve at the deformation temperature of 440°C and the strain rate of 0.1 /s ($\boldsymbol{\Delta}^*$=1.60, $\boldsymbol{\mu_1}$=0.45, $\boldsymbol{\mu_2}$=0.15)

Fig. 12 shows the effect of the damage rate exponent ϕ on the predicted forming limit curve. The shape of a forming limit curve changes dramatically when the value of ϕ varies from 2.0 to 10.0. A parabolic shape of a forming limit curve can be modelled with a high value of ϕ. Two intersection points can be observed on the left and right hand sides of the FLD at β=-0.5 and β=0.2 with fixed parameters of Δ^*, μ_1 and μ_2 at specified values.

5.3 Determination of the constitutive equations

This set of non-linear ordinary differential equations can be solved with the numerical Euler integration method by giving initial values for the variables. The trial and error method was adopted. Material constants of the unified constitutive equations within the Eqns. (3-20) can be determined by fitting the computed true stress-true strain curves to corresponding experimental data obtained from uniaxial tension testing and by fitting computed FLD to corresponding FLD testing results at different deformation temperatures and strain rates after heating and cooling. The first step of the fitting procedure was to determine Eqns. (3)-(8) by taking the temperature dependent parameters as constants for fitting to computed true stress-true strain

curves obtained for different strain rates in uniaxial tensile tests [52]. All the values obtained from the first step were retained in the second step and only the temperature dependent parameters were adjusted. This step was to determine the pre-exponent and activation energy associated constants in Eqns. (9)-(17) by fitting the true stress-true strain curves for different deformation temperatures. Since a forming limit curve represents the onset of localised necking, instead of strain to failure, the value of damage is assumed to be 0.3 when the onset of necking occurs during the calculation process, at which the values of major strain ε_1 and minor strain ε_2 were output. The values of constants in Eqns. (18)-(20) were adjusted until fitting experimental and computed FLD data for different temperatures and strain rates.

The uniaxial tensile test data [52] was used to determine the viscoplastic flow of the material and the calibrated material constants from that for AA6082 under HFQ® conditions are listed in Table 3. The material constants in Eqns. (18)-(20) are determined by fitting the computed FLD to experimental results obtained using the novel biaxial tensile testing system, as listed in Table 4. Fig. 13 shows a comparison between experimental (symbols) and computed (solid curves) FLD using material constants in Table 3 and Table 4 for AA6082 under HFQ® conditions. Good agreement can be seen for each forming limit curve in the diagrams, which indicates that the thermal-activated mechanisms described by Arrhenius-type Eqns. (9)-(20) are applicable for the principal strain-based damage evolution equation and this set of constitutive equations can be used for formability prediction of AA6082 under hot stamping conditions.

Table 3 Material constants for Eqns. (3)-(17) for AA6082 under HFQ® conditions

K_0 (MPa)	k_0 (MPa)	n_{0_1}	B_0 (MPa)	C_0	η_{1_0}	η_{2_0}
0.3624	0.5897	0.1018	4.8251	7.3057	2.4577	0.8357
η_{3_0}	E_0 (MPa)	A	n_2	Q_K (J/mol)	Q_k (J/mol)	Q_{n1} (J/mol)
0.2423	249.69	0.19	1.83	25409.54	21692.97	17637.07
Q_B (J/mol)	Q_C (J/mol)	$Q_{\eta1}$ (J/mol)	$Q_{\eta2}$ (J/mol)	$Q_{\eta3}$ (J/mol)	Q_E (J/mol)	R (J/(molK))
15698.86	2112.59	16273.24	837.80	22107.92	27987.42	8.314

Table 4 Material constants for Eqns. (18)-(20) for AA6082 under HFQ® conditions

μ_{11}	μ_{12}	μ_2	ϕ_{11}	ϕ_{12}
0.848	451.863	0.150	19.094	874.552
Δ_{11}^*	Δ_{12}^*	Δ_{21}^*	Δ_{22}^*	γ
79.785	26.063	-81.107	3.517E-03	0.0035

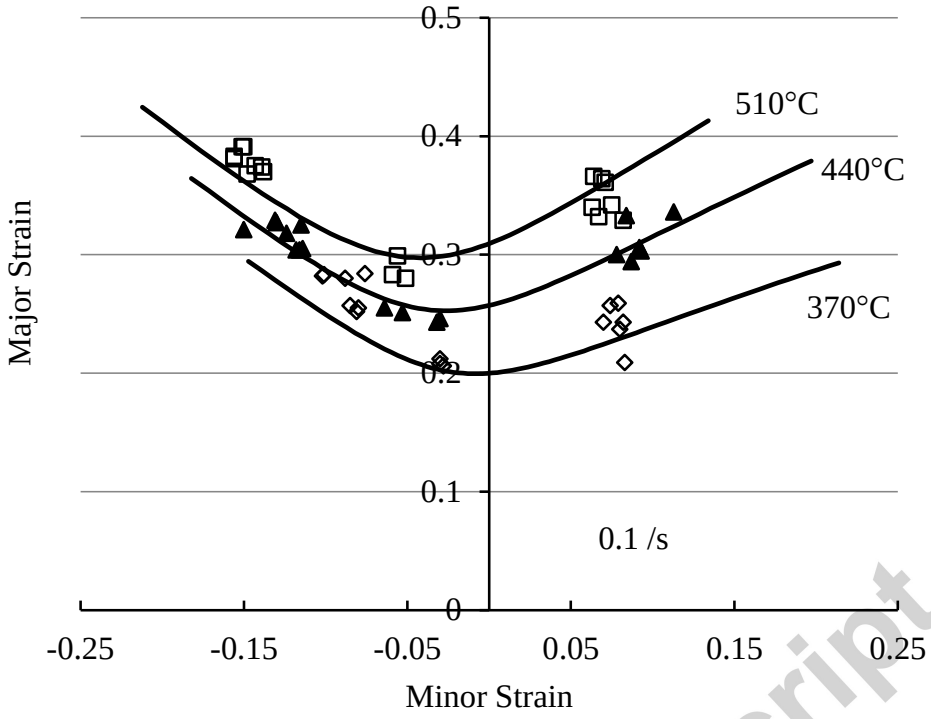

(a) FLD for different deformation temperatures at 0.1 /s

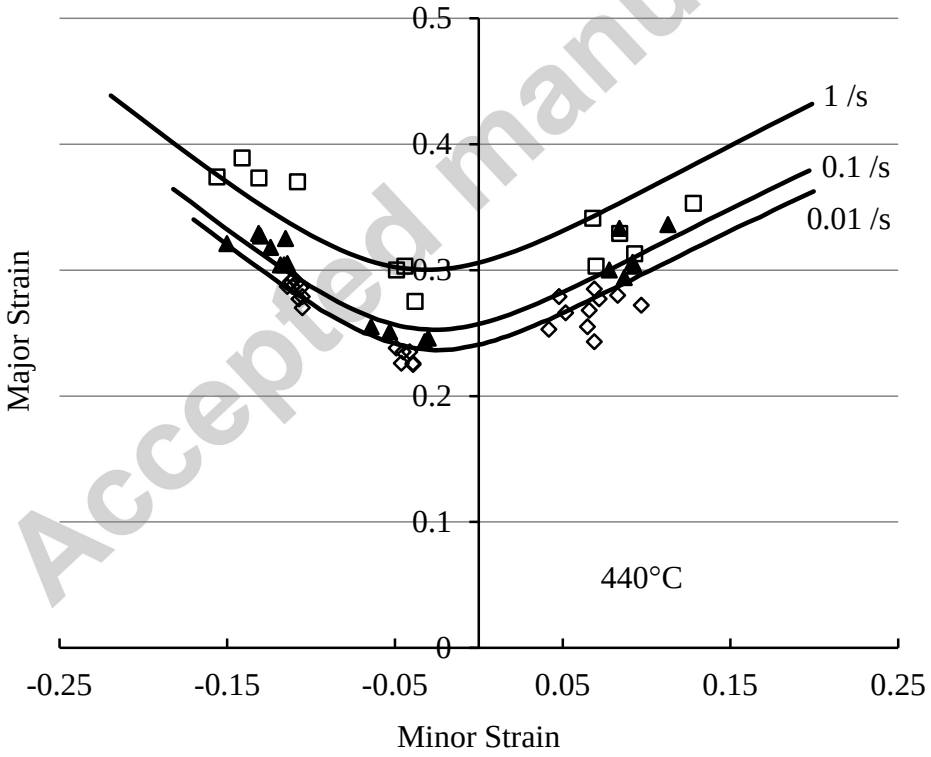

(b) FLD for different strain rates at 440°C

Fig.13 Comparison of experimental (symbols) and numerically predicted (solid curves) FLDs computed using the 2D CDM-based materials model for AA6082 with various deformation temperatures and strain rates

To validate the determined material model, further tests were carried out at the deformation temperature of 510°C at different strain rates under HFQ® conditions and the results are shown in Fig. 14. Computations were carried out at the test conditions. The good agreement between the experimental and computational results shows the capability and the validation of the material model for hot stamping applications.

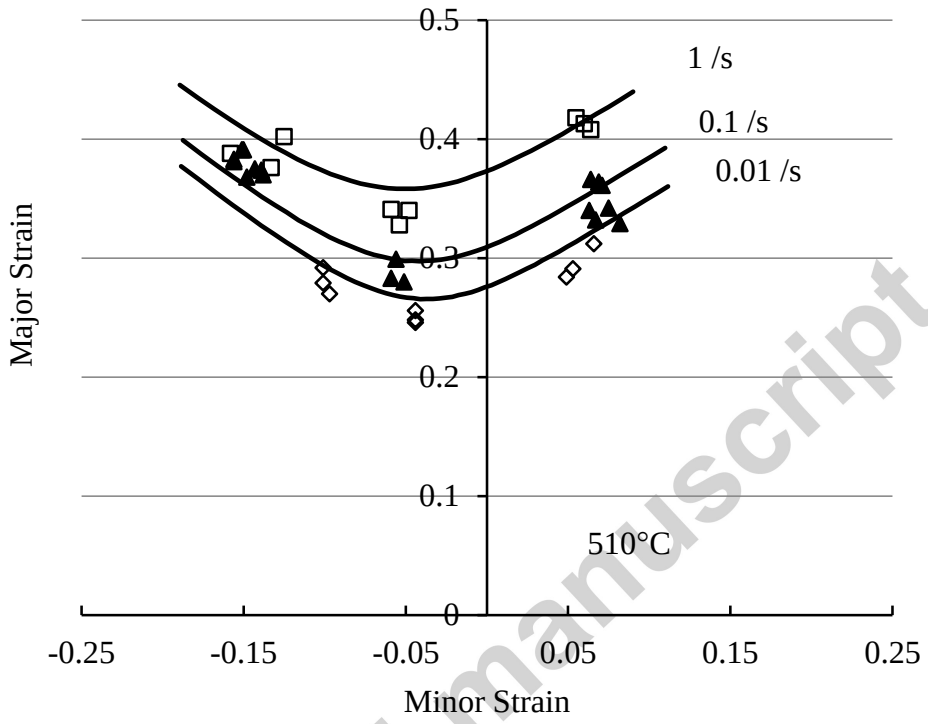

Fig.14 Validation of the determined CDM-based materials model for AA6082 by comparing experimental (symbols) and numerically predicted (solid curves) FLDs at the deformation temperatures of 510°C

6. Conclusions

A set of unified viscoplastic-damage constitutive equations was adopted to model the thermo-mechanical response and formability of sheet metals under a range of forming temperatures and strain rates. This 2D CDM based material model was developed to predict the formability of AA6082 sheet under HFQ® conditions. The predicted shape and position of forming limit curves in an FLD can be controlled by parameters in the damage evolution equation.

In order to determine FLDs at elevated temperatures for application to hot sheet stamping conditions, a novel planar biaxial testing system was designed, using resistance heating and air cooling on a Gleeble materials simulator machine. Designed uniaxial and cruciform specimens were used to conduct formability tests at designated

deformation temperatures (370-510°C) and strain rates (0.01-1 /s) after heating and rapid cooling processes. The FLDs of AA6082 under HFQ® conditions were determined at the first time and it is found that forming limit increases with increasing strain rate (0.01-1 /s) and increasing temperature (370-510°C).

Material constants have been calibrated and validated from experimental FLD results of AA6082. Good agreement between each set of experimental and predicted FLD data has been obtained, which means that this set of viscoplastic damage constitutive equations is able to predict the damage evolution process and the failure of an alloy under hot stamping conditions. The formability of the sheet metal under hot stamping conditions was evaluated, for the first time, by the proposed material modelling technique. The experimental and modelling techniques could be applied to other sheet metals for hot stamping applications.

Acknowledgements

Financial support from Impression Technologies Ltd for this research project is gratefully acknowledged by the authors. In addition, this research was supported by the European Union's Seventh Framework Programme (FP7/2007-2013) under grant agreement No. 604240, project title 'An industrial system enabling the use of a patented, lab-proven materials processing technology for Low Cost forming of Lightweight structures for transportation industries (LoCoLite)'.

References

[1] Z. Shao, N. Li, J. Lin, T.A. Dean, Development of a New Biaxial Testing System for Generating Forming Limit Diagrams for Sheet Metals Under Hot Stamping Conditions, Experimental Mechanics, 56 (2016) 1489-1500.
[2] W.S. Miller, L. Zhuang, J. Bottema, A.J. Wittebrood, P. De Smet, A. Haszler, A. Vieregge, Recent development in aluminium alloys for the automotive industry, Materials Science and Engineering, 280 (2000) 37-49.
[3] N.P. Lutsey, Review of technical literature and trends related to automobile mass-reduction technology, in: Institute of Transportation Studies, University of California, 2010.
[4] R. George, A. Bardelcik, M.J. Worswick, Hot forming of boron steels using heated and cooled tooling for tailored properties, Journal of Materials Processing Technology, 212 (2012) 2386-2399.
[5] A. Foster, T.A. Dean, J. Lin, Process for forming aluminium alloy sheet component, in: U.P. Office (Ed.) UK Patent Office, UK, 2012.
[6] H. Karbasian, A.E. Tekkaya, A review on hot stamping, Journal of Materials Processing Technology, 210 (2010) 2103-2118.

[7] O. El Fakir, L. Wang, D. Balint, J.P. Dear, J. Lin, T.A. Dean, Numerical study of the solution heat treatment, forming, and in-die quenching (HFQ) process on AA5754, International Journal of Machine Tools and Manufacture, 87 (2014) 39-48.
[8] O. El Fakir, S. Chen, L.L. Wang, D. Balint, J.P. Dear, J.G. Lin, Numerical Investigation on the Hot Forming and Cold-Die Quenching of an Aluminium-Magnesium Alloy into a Complex Component, Materials Science Forum, 765 (2013) 368-372.
[9] J. Lin, T.A. Dean, R.P. Garrett, A process in forming high strength and complex-shaped Al-alloy sheet components, in: B. Patent (Ed.) UK Patent UK, 2008.
[10] M.S. Mohamed, A.D. Foster, J. Lin, D.S. Balint, T.A. Dean, Investigation of deformation and failure features in hot stamping of AA6082: Experimentation and modelling, International Journal of Machine Tools and Manufacture, 53 (2012) 27-38.
[11] J. Lin, T.A. Dean, A.D. Foster, L. Wang, D. Balint, A method of forming a component of complex shape from aluminium alloy sheet, in: U. patent (Ed.) UK patent UK, 2011.
[12] S.P. Keeler, W.A. Backofen, Plastic instability and fracture in sheets stretched over rigid punches, ASM Transactions Quarterly, 56 (1963) 25-48.
[13] A. Graf, W. Hosford, The influence of strain-path changes on forming limit diagrams of A1 6111 T4, International Journal of Mechanical Sciences, 36 (1994) 897-910.
[14] T.B. Stoughton, J.W. Yoon, Sheet metal formability analysis for anisotropic materials under non-proportional loading, International Journal of Mechanical Sciences, 47 (2005) 1972-2002.
[15] K. Nakazima, T. Kikuma, K. Hasuka, Study on the formability of steel sheets, in: Yawata Technical Report 264, 1968, pp. 8517–8530.
[16] A.J. Ranta-Eskola, Use of the hydraulic bulge test in biaxial tensile testing, International Journal of Mechanical Sciences, 21 (1979) 457-465.
[17] T. Kuwabara, F. Sugawara, Multiaxial tube expansion test method for measurement of sheet metal deformation behavior under biaxial tension for a large strain range, International Journal of Plasticity, 45 (2013) 103-118.
[18] K. Liu, L. Lang, G. Cai, X. Yang, C. Guo, B. Liu, A novel approach to determine plastic hardening curves of AA7075 sheet utilizing hydraulic bulging test at elevated temperature, International Journal of Mechanical Sciences, 100 (2015) 328-338.
[19] R.A. Ayres, M.L. Wenner, Strain and strain-rate hardening effects in punch stretching of 5182-0 aluminum at elevated temperatures, Metallurgical Transactions A, 10 (1979) 41-46.
[20] R. Bagheriasl, Formability of Aluminum Alloy Sheet at Elevated Temperature, in, University of Waterloo, 2012.
[21] N.A. Sène, P. Balland, R. Arrieux, K. Bouabdallah, An Experimental Study of the Microformability of Very Thin Materials, Experimental Mechanics, 53 (2012) 155-162.
[22] J. Min, J. Lin, Y. Cao, W. Bao, Z. Lu, Effect of necking types of sheet metal on the left-hand side of forming limit diagram, Journal of Materials Processing Technology, 210 (2010) 1070-1075.
[23] Z. Shao, Q. Bai, N. Li, J. Lin, Z. Shi, M. Stanton, D. Watson, T. Dean, Experimental investigation of forming limit curves and deformation features in warm forming of an aluminium alloy, Proceedings of the Institution of Mechanical Engineers, Part B: Journal of Engineering Manufacture, (2016).
[24] Z. Marciniak, K. Kuczynski, Limit strains in the processes of stretch-forming sheet metal, International Journal of Mechanical Sciences, 9 (1967) 609-620.

[25] D. Li, A.K. Ghosh, Biaxial warm forming behavior of aluminum sheet alloys, Journal of Materials Processing Technology, 145 (2004) 281-293.
[26] T. Naka, G. Torikai, R. Hino, F. Yoshida, The effects of temperature and forming speed on the forming limit diagram for type 5083 aluminium-magnesium alloy sheet, Journal of Materials Processing Technology, 113 (2001) 648-653.
[27] A. Hannon, P. Tiernan, A review of planar biaxial tensile test systems for sheet metal, Journal of Materials Processing Technology, 198 (2008) 1-13.
[28] L. Leotoing, D. Guines, I. Zidane, E. Ragneau, Cruciform shape benefits for experimental and numerical evaluation of sheet metal formability, Journal of Materials Processing Technology, 213 (2013) 856-863.
[29] L. Leotoing, D. Guines, Investigations of the effect of strain path changes on forming limit curves using an in-plane biaxial tensile test, International Journal of Mechanical Sciences, 99 (2015) 21-28.
[30] I. Zidane, D. Guines, L. Léotoing, E. Ragneau, Development of an in-plane biaxial test for forming limit curve (FLC) characterization of metallic sheets, Measurement Science and Technology, 21 (2010) 055701.
[31] F. Abu-Farha, L.G. Hector Jr., M. Khraisheh, Cruciform-shaped specimens for elevated temperature biaxial testing of lightweight materials, JOM, 61 (2009).
[32] D. Banabic, F. Barlat, O. Cazacu, T. Kuwabara, Advances in anisotropy and formability, International Journal of Material Forming, 3 (2010) 165-189.
[33] T.B. Stoughton, X. Zhu, Review of theoretical models of the strain-based FLD and their relevance to the stress-based FLD, International Journal of Plasticity, 20 (2004) 1463-1486.
[34] P. Hora, L. Tong, Prediction of forming limits in virtual sheet metal forming– yesterday, today and tomorrow, in: Proceedings of the FLC, Zurich, 2006, pp. 8-23.
[35] P. Hora, M. Merklein, L. Tong, J. Lechler, Numerical and experimental evaluation of thermal dependent FLC (FLC-T), in: IDDRG 2007 International Conference, Hungary, 2007, pp. 23-30.
[36] N. Abedrabbo, F. Pourboghrat, J. Carsley, Forming of aluminum alloys at elevated temperatures – Part 1: Material characterization, International Journal of Plasticity, 22 (2006) 314-341.
[37] N. Abedrabbo, F. Pourboghrat, J. Carsley, Forming of aluminum alloys at elevated temperatures – Part 2: Numerical modeling and experimental verification, International Journal of Plasticity, 22 (2006) 342-373.
[38] S. Stören, J.R. Rice, Localized necking in thin sheets, Journal of the Mechanics and Physics of Solids, 23 (1975) 421–441.
[39] J. Min, J. Lin, J. Li, W. Bao, Investigation on hot forming limits of high strength steel 22MnB5, Computational Materials Science, 49 (2010) 326-332.
[40] J. Lin, A.D. Foster, Y. Liu, D.C.J. Farrugia, T.A. Dean, On micro-damage in hot metal working part 2: constitutive modelling, Engineering transactions, 55 (2007) 43-60.
[41] M. Mohamed, Z.S. Shi, J.G. Lin, T. Dean, J. Dear, Strain-Based Continuum Damage Mechanics Model for Predicting FLC of AA5754 under Warm Forming Conditions, Applied Mechanics and Materials, 784 (2015) 460-467.
[42] M. Rodríguez-Millán, A. Vaz-Romero, A. Rusinek, J.A. Rodríguez-Martínez, A. Arias, Experimental Study on the Perforation Process of 5754-H111 and 6082-T6 Aluminium Plates Subjected to Normal Impact by Conical, Hemispherical and Blunt Projectiles, Experimental Mechanics, 54 (2014) 729-742.

[43] R. Garrett, J. Lin, T. Dean, An investigation of the effects of solution heat treatment on mechanical properties for AA 6xxx alloys: experimentation and modelling, International Journal of Plasticity, 21 (2005) 1640-1657.
[44] B. Milkereit, N. Wanderka, C. Schick, O. Kessler, Continuous cooling precipitation diagrams of Al–Mg–Si alloys, Materials Science and Engineering: A, 550 (2012) 87-96.
[45] J. Coër, C. Bernard, H. Laurent, A. Andrade-Campos, S. Thuillier, The Effect of Temperature on Anisotropy Properties of an Aluminium Alloy, Experimental Mechanics, 51 (2010) 1185-1195.
[46] A. Makinde, L. Thibodeau, K.W. Neale, Development of an apparatus for biaxial testing using cruciform specimens, Experimental mechanics 32 (1992) 138-144.
[47] M. Kosai, A. Shimamoto, C. Yu, A. Kobayashi, P. Tan, A biaxial test specimen for crack arrest studies, Experimental mechanics, 36 (1996) 277-283.
[48] Y. Yu, M. Wan, X.-D. Wu, X.-B. Zhou, Design of a cruciform biaxial tensile specimen for limit strain analysis by FEM, Journal of Materials Processing Technology, 123 (2002) 67-70.
[49] D.A. Kelly, Problems in creep testing under biaxial stress systems, The Journal of Strain Analysis for Engineering Design, 11 (1976) 1-6.
[50] D.R. Hayhurst, A biaxial-tension creep-rupture testing machine, The Journal of Strain Analysis for Engineering Design, 8 (1973) 119-123.
[51] Metallic materials-sheet and strip-determination of forming limit curves, Part 2: Determination of forming limit curves in the laboratory, in, International Organization for Standardization, 2004.
[52] N. Li, Z. Shao, J. Lin, T.A. Dean, Investigation of Uniaxial Tensile Properties of AA6082 under HFQ® Conditions, Key Engineering Materials, 716 (2016) 337-344.
[53] J. Lin, Fundamentals of materials modelling for metals processing technologies: theories and applications, Imperial college press, 2015.
[54] J. Lin, M. Mohamed, D. Balint, T. Dean, The development of continuum damage mechanics-based theories for predicting forming limit diagrams for hot stamping applications, International Journal of Damage Mechanics, 23 (2013) 684-701.
[55] M.A. Khaleel, H.M. Zbib, E.A. Nyberg, Constitutive modeling of deformation and damage in superplastic materials, International Journal of Plasticity, 17 (2001) 277-296.

Highlights:

1. A novel biaxial testing system was developed for hot stamping applications.
2. FLDs of AA6082 were obtained at various temperatures and strain rates.
3. Unified viscoplastic constitutive equations were proposed to predict formability.
4. Constitutive equations were determined and verified through experimental results.